Eidgenössische Technische Hochschule Zürich Swiss Federal Institute of Technology Zurich

Genehmigung des Forschungsplans

(Definitive Zulassung zum Doktorat)

Approval of the Research Plan

(Full admission to doctoral studies)

Studierenden-Nummer student number	17	902	- -	594	
Name family name	Sinkunaite	e			
Vorname first name	Laura Pau	ılina			
Departement department	D - PHY	S			
Der Forschungsplan w The research plan has Name Doktorand/in Name of doctoral student					und angenommen durch: roved by: Unterschrift Signature
Name Dissertationsleiter/in Name of supervisor		Datum Date			Unterschrift Signature
Name Bevollmächtigter Doktora Name of representative of doct		Datum Date			Unterschrift Signature

Für Kandidaten mit Zulassungsprüfung/en:

Die Zulassungsprüfung/en müssen vor Genehmigung des Forschungsplans erfüllt sein!

For candidates who have to fulfil further conditions of admission: These conditions must be fulfilled **before** the research plan can be approved!

Frist für Einreichung des Forschungsplans

Frühestens nach erfüllen und offiziell verfügtem Bestehen der Zusatzbedingungen, spätestens ein Jahr nach der Einschreibung

Vorgehen zur Genehmigung des Forschungsplans

Lassen Sie dieses Formular und den Forschungsplan von Ihrer Leiterin / Ihrem Leiter unterzeichnen und senden Sie danach beides an das zuständige **Studiensekretariat**. Dieses kümmert sich um die Unterschrift des Bevollmächtigten des Doktoratsausschusses und schickt das Formular anschliessend an die Doktoratsadministration.

Deadline for submission of the research plan

Only after having passed and received official notification of having successfully fulfilled the further conditions of admission, one year after registration at the latest

Procedure for approval of your research plan

Please ask your supervisor to sign this form and your research plan and send both to the **Study Administration Office of your department**. They will take care of having it signed by the representative of the doctoral board and will forward it to the Doctoral Administration Office afterwards.



Research Plan

Doctoral thesis:

The detection system for the HyperMu experiment Doctoral thesis title (provisional)

01.11.2017

Beginning date of doctoral thesis

Doctoral student:

17-902-594

Student number

Laura Paulina Sinkunaite

Name

laura-paulina.sinkunaite@psi.ch

E-mai

Paul Scherrer Institut

Institution (if external doctoral thesis)

Date, signature

Supervisor:

Prof. Dr. Klaus Kirch

Name, title

Date, signature

Co-examiner (if already known):

Name, title

Affiliation

E-mai

Please hand in this form together with the research plan and the form "Approval of the research plan" to the Doctoral Administration Office of D-PHYS

Research Plan

for a Doctoral Study in Physics at the D-PHYS of ETH Zurich

Laura Paulina Šinkūnaitė

1 Introduction and motivation

Proton-radius puzzle The previously conducted measurements [1], [2] of the 2S-2P energy splitting in muonic hydrogen (μp) from the triplet $(2S_{1/2}^{F=1}-2P_{3/2}^{F=2})$ and the singlet $(2S_{1/2}^{F=0}-2P_{3/2}^{F=1})$ 2S sub-levels have shown a 7σ discrepancy comparing to the values extracted from the electron-proton scattering and hydrogen (H) spectroscopy. This so-called "proton-radius puzzle" is interesting for different areas of physics research: verifications of the proton structure at low energies, new determinations of the Rydberg constant, and searches of BSM physics. Moreover, it has triggered various reanalysis of electron-proton scattering data and several new experiments in the field of scattering and atomic physics. So far, the resolution of the "proton-radius puzzle" remains unknown.

Hyperfine splitting The Hyperfine splitting (HFS) is the magnetic moment - magnetic moment interaction. This can be described [3] as

$$\Delta E_{theor}^{HFS} = E^F (1 + \Delta_{QED} + \Delta_{TPE} + \Delta_{weak+HVP}), \tag{1}$$

with E^F denoting the Fermi energy

$$E^F = \frac{8}{3}\alpha^4 \frac{\mu_p m_1^2 m_2^2}{(m_1 + m_2)^3},\tag{2}$$

 Δ_{TPE} the two-photon exchange (TPE) contribution (Fig. 1), α the fine-structure constant, μ_p the proton magnetic moment, m_1 the muon mass, and m_2 the proton mass. Δ_{QED} represents the QED contribution, $\Delta_{weak+HVP}$ denotes the contribution of hadronic vacuum polarisation and weak interaction, and Δ_{TPE} is the correction due to the proton structure [4].

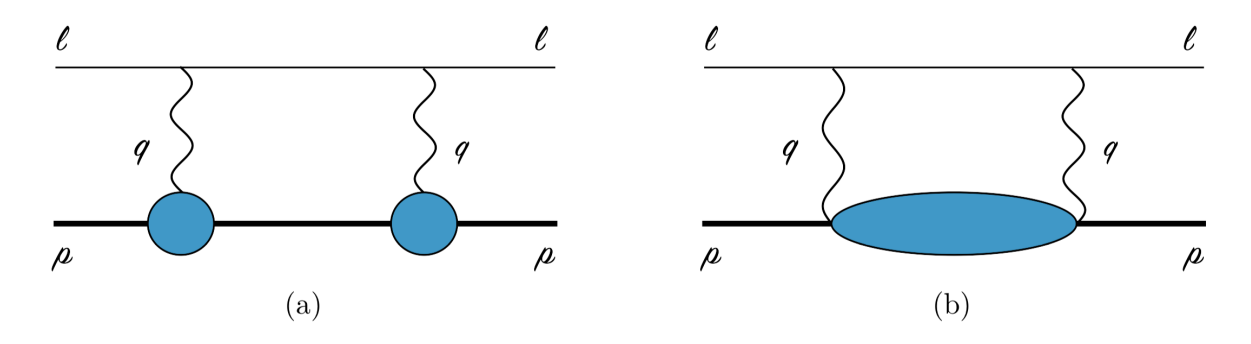


Figure 1: TPE diagrams: the horizontal lines correspond to the lepton and the nucleus (bold). (a) Elastic contribution to the TPE diagram. (b) Inelastic contribution to the TPE diagram, where the "blob" represents all possible excitations [5].

Two-photon exchange The TPE can be divided into 3 terms,

$$\Delta_{TPE} = \Delta_Z + \Delta_{recoil} + \Delta_{pol},\tag{3}$$

where the elastic contribution (Zemach) is given by

$$\Delta_Z = \frac{8Z\alpha m_r}{\pi} \int_0^\infty \frac{dQ}{Q^2} \left(G_E(Q^2) \frac{G_M(Q^2)}{1 + \kappa_p} - 1 \right) = -2(Z\alpha) m_r R_Z, \tag{4}$$

with the Zemach radius defined as

$$R_Z = -\frac{4}{\pi} \int_0^\infty \frac{dQ}{Q^2} \left(G_E(Q^2) \frac{G_M(Q^2)}{1 + \kappa_p} - 1 \right), \tag{5}$$

where κ_p is a term related to the dipole magnetic moment of the proton. The Zemach radius non-relativistically reduces to the convolution of charge ρ_E and magnetic ρ_M distributions

$$R_Z = \int d^3 \mathbf{r} |\mathbf{r}| \int d^3 \mathbf{r'} \rho_E(\mathbf{r} - \mathbf{r'}) \rho_M(\mathbf{r'}). \tag{6}$$

This is the contribution with the largest uncertainty of the order of 1×10^{-4} of the total HFS. The Δ_{pol} term is the polarisability contribution and the Δ_{recoil} is the negligible recoil correction to the Zemach term. There are two approaches to evaluate the polarisability contribution: using dispersion relations and data such as structure functions and form factors or using chiral perturbation theory. In the dispersive approach, the inelastic contribution can be fully calculated using the measured spin-dependent structure functions of the proton, $g_1(x,Q^2)$ and $g_2(x,Q^2)$ [3].

Motivation The measurement of the 1S-HFS transition in the μp with 1 ppm accuracy can be used to evaluate the TPE contribution with a relative accuracy of 1×10^{-4} . This would increase our understanding of the low-energy structure of the proton and would provide a benchmark for chiral perturbation theory, dispersion-based approaches, and lattice QCD. A new experiment (HyperMu) designed to contribute to the resolution of the "proton-radius puzzle" is being developed at the Paul Scherrer Institute (PSI). HyperMu is aiming to measure the ground-state hyperfine splitting (1S-HFS) in μp (Fig. 2) with an accuracy of 1 ppm by means of laser spectroscopy. From the successful measurement of the 1S-HFS transition, the nuclear-structure - related Δ_{TPE} contribution effects can be determined with a relative accuracy of 1×10^{-4} . In a second step from the TPE, the Zemach radius can be extracted to accuracies of about $\mathcal{O}(10^{-3})$ limited by the theoretical uncertainty of the polarisability contribution. Moreover, the measurement would also be a test of the lepton universality, i.e. when μp laser spectroscopy results are compared to the electron-proton scattering and to the electronic hydrogen (ep) spectroscopy, and on top of that it would impact the resolution of the "proton radius puzzle" and the related "new physics" searches.

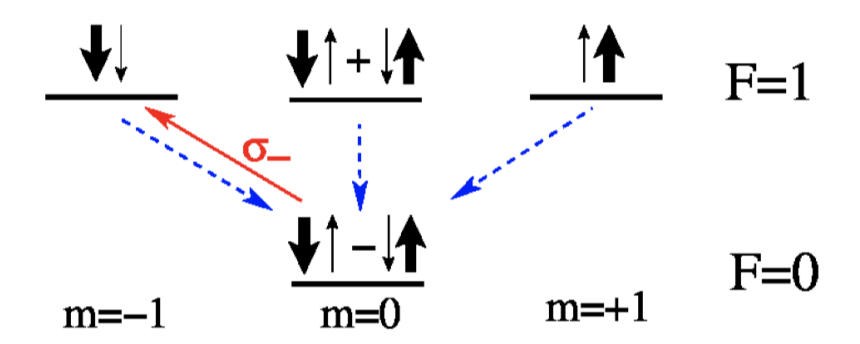


Figure 2: Energy levels and spin compositions of the 1S states in μp . The red arrow represents the transition driven by the circularly polarised laser light, the blue arrows illustrate the collisional quenching [3].

2 Working principle

The principle of the HyperMu experiment: Muons are stopped in hydrogen gas forming μp atoms in highly-excited states. The formed μp atoms de-excite to the F=0 sub-level of the ground state (Fig. 2). A high-energy laser pulse (3 mJ at $6.7\mu m$ and 100 MHz bandwidth) excites the μp atoms to the F=1 sub-level of the ground state,

$$\mu p_{F=0} + \gamma \rightarrow \mu p_{F=1}$$
.

In collisions with hydrogen molecules (H_2) , the μp atoms are de-excited to the F=0 sub-level,

$$\mu p_{F=1} + H_2 \rightarrow \mu p_{F=0} + H_2 + E_{kin}$$
.

This transition energy is converted into the kinetic energy. Having this extra kinetic energy, the μp atoms efficiently diffuse to the target walls before muon decays occur. At the target wall, which is made of the high-Z material, the muons are transferred from the μp to the high-Z material forming $(\mu Z)^*$ in an excited state. The highly-excited $(\mu Z)^*$ atoms then de-excite producing MeV X-rays. The MeV X-rays are detected using scintillating detectors (Fig. 3). A resonance curve is obtained by plotting the number of the X-rays versus the laser frequency.

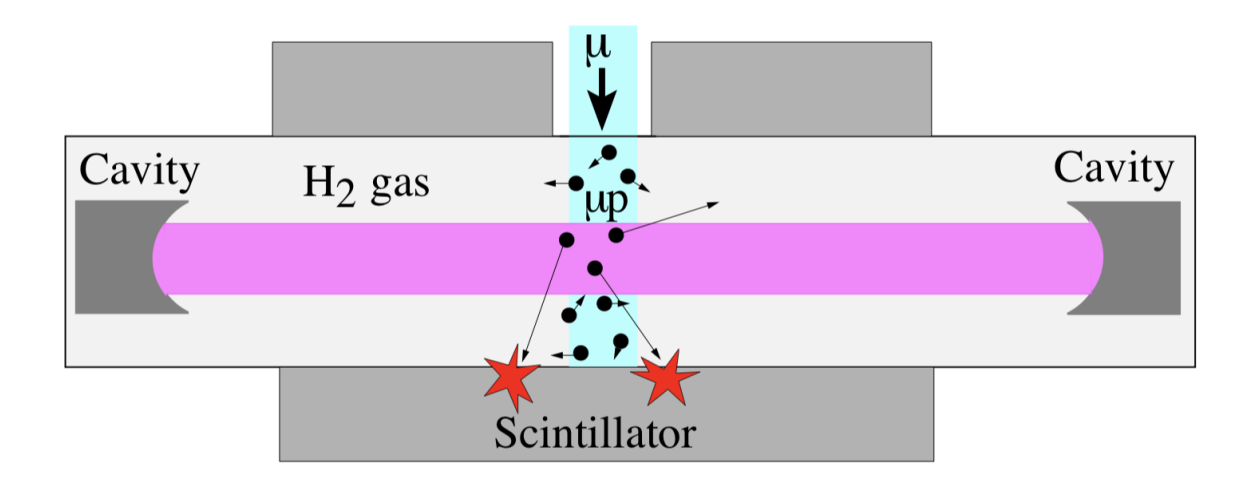


Figure 3: HyperMu experimental scheme showing a laser cavity, muon entrance beam, and the surrounding scintillating detectors [3].

Signal and background The signal events are considered to be the MeV X-rays detected within a time window Δt after the laser excitation. There are two types of background events: intrinsic and erroneous. The intrinsic background is produced by non-laser excited μp atoms, that diffuse to the target walls in the observation time window Δt . This type of background can be minimised by cooling down the target, e.g. keeping the H_2 gas at 50 K temperature. The other type of background arises from the electrons produced in the event of a muon decay, $\mu^- \to e^- + \overline{\nu_e} + \nu_\mu$, and being falsely identified as X-rays.

Laser system To produce a resonance curve for the 1S-HFS transition in the μp , a high-energy laser system delivering 3 mJ pulses with 100 MHz bandwidth at 6.7 μm is needed. We are planning to realise a laser system as depicted in Fig. 4. It is composed of a thin-disk laser followed by optical-parametric down-conversion stages (OPO - OPA) and a difference frequency generating stage (DFG). Using this OPO and OPA scheme, the thin-disk laser needs to be operated in single-frequency mode achieved by injection seeding the thin-disk laser oscillator with an external frequency stabilised continuous-wave (cw) laser at 1030 nm. The pulses

at 1030 nm would then be down-converted in a non-linear crystal to produce two beams, so called an "idler" beam at 2434 nm and a "signal" beam at 1785 nm. The OPO cavity needs to be seeded by a tunable "signal" laser used to scan the resonance. A successive difference frequency generation (DFG) between "idler" and "signal" pulses would then be used to generate 3 mJ pulses at 6.7μ m.

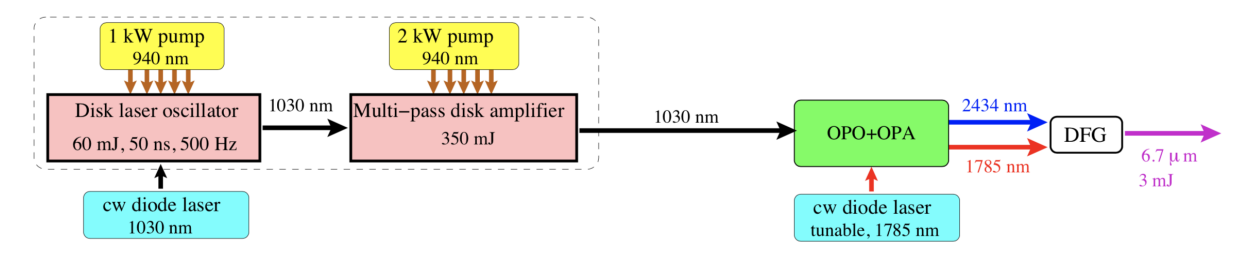


Figure 4: Possible parametric down-conversion laser scheme for μp experiment using OPO and OPA technologies [3].

3 The detection system

Requirements One of the main topics of this thesis is to develop the needed detection system for the HFS experiment. The aims of the detection system are listed below.

- 1. Detection of the incoming muons. The detected signal is used to trigger the Data Acquisition (DAQ) and the laser systems.
- 2. Measurement of the produced X-ray cascades in the $(\mu Z)^*$ de-excitation process after the μp atoms have diffused to the target wall.
- 3. Detection of the nuclear capture event. After de-excitation to the ground-state, the muons in the μZ atoms are mainly captured in the nuclear process $(\mu^- + p \rightarrow n + \nu_\mu)$.
- 4. The detection system also needs to measure the electrons from regular muon decays. Those electrons are produced mainly by the μp atoms formed in the hydrogen gas that

decay have not reached the target wall. Note that the nuclear capture rate in the μp atom is much smaller than in high-Z μZ atoms.

5. The detection system must also deal with the background coming from the beam-line and muons stopping in the entrance detector and target window.

For simplicity, in this plan we will only describe the detection of electrons coming from the muon decays and X-rays coming from the muonic X-ray cascade (Table 1).

Detectors The ideal detector for measuring the muonic X-rays would be germanium (Ge) as it provides an excellent energy resolution. However, its detection rate (possible solid angle coverage) is too low for HyperMu. Therefore, we need to use alternative detectors that could fulfil the following conditions.

- i. High detection efficiency for cascade ($\geq 50\%$) and electron, and the ability to distinguish between them (the false identification of electrons as X-rays should be $< 5 \times 10^{-3}$). Time resolutions must be of about 10 ns. We are considering to use thin plastic scintillators to distinguish between X-ray from the cascade event and an electron from the muon decay (Fig. 7). The energy spectrum of cascade events differs considerably from the energy spectrum of an electron from muon decay.
- ii. Indeed, during a cascade process several X-rays are produced (see Table 1) with total energy of about 10 MeV. Since only a fraction of these X-rays (and energy) is detected in the scintillator, a complex measurable energy spectrum is obtained with an "endpoint" energy of 10 MeV (see Fig. 7). Therefore, a simple energy cut could be used to partially sort out between e^- and X-rays.

The energy spectrum of the emitted electron from muon decay is shown in Fig. 5. Electrons up to the energies of 50 MeV are emitted in the muon decay. A considerable fraction is above

10 MeV. So these events which deposit more than 10 MeV energy in the scintillator can be identified as "electrons". Therefore, a simple energy cut could be used to partially sort out between e^- and X-rays.

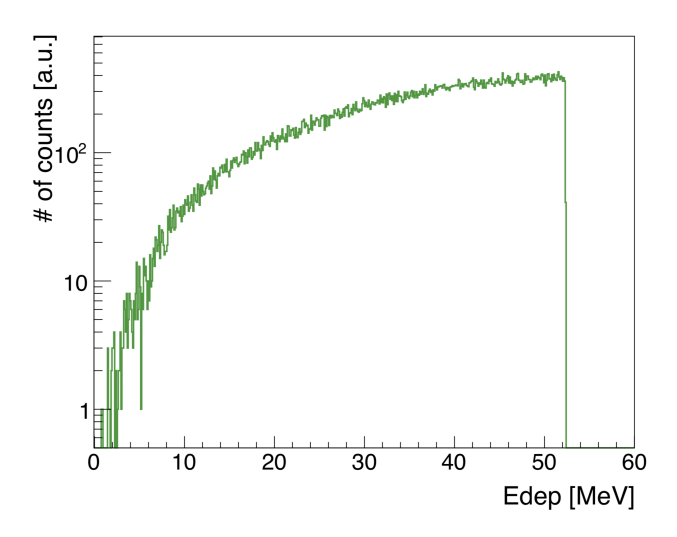


Figure 5: Michel decay spectrum for a muon.

Signal to background ratio In this sub-section we briefly motivate the requirements that the false identification of e^- as cascade events should have a probability smaller than 5×10^{-3} . This requirement can be estimated by calculating the number of μp atoms which are in the hydrogen gas target and decay in the event time window $\Delta t \sim 300$ ns following the laser excitation, and by comparing it to the number of μp atoms that after the laser-excitation reach the target walls in the observation time window Δt . Then the number of muon decay in the observation time window $\Delta t = 300$ ns (see Fig. 6) can be expressed as

$$B \approx d\left(\frac{A_2}{A_1}\right) N_{stopped \,\mu^-} P_{\mu^- \to e^- \overline{\nu_e} \nu_\mu} \varepsilon_{det,e^-} = d\left(\frac{A_2}{A_1}\right) N_{stopped \,\mu^-} \left(1 - e^{-\frac{300ns}{2200ns}}\right) \varepsilon_{det,e^-}, \quad (7)$$

where d is the target length, the ratio $\frac{A_2}{A_1}$ represents the μp density loss in the time between the muonic atom formation and the base excitation, $P_{\mu^- \to e^- \overline{\nu_e} \nu_\mu}$ is the probability for a muon

Table 1: X-ray transitions in gold

	Relative probability [%] 90.00 4.50 0.30 0.10 1.00 84.00 6.00 1.11 0.40 0.25 76.00	5.65 8.10 9.00 9.40 9.60 2.40 3.30 3.70 3.90 4.20
$3 \rightarrow 1$ $4 \rightarrow 1$ $5 \rightarrow 1$ $> 6 \rightarrow 1$ $3 \rightarrow 2$ $4 \rightarrow 2$ $5 \rightarrow 2$ $6 \rightarrow 2$ $> 7 \rightarrow 2$ $4 \rightarrow 3$ $5 \rightarrow 3$	4.50 0.30 0.10 1.00 84.00 6.00 1.11 0.40 0.25 76.00	8.10 9.00 9.40 9.60 2.40 3.30 3.70 3.90 4.20
$4 \rightarrow 1$ $5 \rightarrow 1$ $> 6 \rightarrow 1$ $3 \rightarrow 2$ $4 \rightarrow 2$ $5 \rightarrow 2$ $6 \rightarrow 2$ $> 7 \rightarrow 2$ $4 \rightarrow 3$ $5 \rightarrow 3$	0.30 0.10 1.00 84.00 6.00 1.11 0.40 0.25 76.00	9.00 9.40 9.60 2.40 3.30 3.70 3.90 4.20
$5 \rightarrow 1$ $> 6 \rightarrow 1$ $3 \rightarrow 2$ $4 \rightarrow 2$ $5 \rightarrow 2$ $6 \rightarrow 2$ $> 7 \rightarrow 2$ $4 \rightarrow 3$ $5 \rightarrow 3$	0.10 1.00 84.00 6.00 1.11 0.40 0.25 76.00	9.40 9.60 2.40 3.30 3.70 3.90 4.20
	1.00 84.00 6.00 1.11 0.40 0.25 76.00	9.60 2.40 3.30 3.70 3.90 4.20
$3 \rightarrow 2$ $4 \rightarrow 2$ $5 \rightarrow 2$ $6 \rightarrow 2$ $> 7 \rightarrow 2$ $4 \rightarrow 3$ $5 \rightarrow 3$	84.00 6.00 1.11 0.40 0.25 76.00	2.40 3.30 3.70 3.90 4.20
$ 4 \rightarrow 2 $ $ 5 \rightarrow 2 $ $ 6 \rightarrow 2 $ $ > 7 \rightarrow 2 $ $ 4 \rightarrow 3 $ $ 5 \rightarrow 3 $	6.00 1.11 0.40 0.25 76.00	3.30 3.70 3.90 4.20
$ 5 \rightarrow 2 $ $ 6 \rightarrow 2 $ $ > 7 \rightarrow 2 $ $ 4 \rightarrow 3 $ $ 5 \rightarrow 3 $	1.11 0.40 0.25 76.00	3.70 3.90 4.20
$ \begin{array}{c} 6 \to 2 \\ > 7 \to 2 \\ \hline 4 \to 3 \\ 5 \to 3 \end{array} $	0.40 0.25 76.00	3.90 4.20
	0.25 76.00	4.20
$\begin{array}{c} 4 \rightarrow 3 \\ 5 \rightarrow 3 \end{array}$	76.00	
$5 \rightarrow 3$		
	0.00	0.90
$6 \rightarrow 3$	8.00	1.30
9 , 9	2.00	1.50
$7 \rightarrow 3$	0.80	1.70
$> 8 \rightarrow 3$	2.50	1.80
$5 \rightarrow 4$	66.00	0.40
$6 \rightarrow 4$	9.00	0.60
$7 \rightarrow 4$	3.00	0.70
$8 \rightarrow 4$	1.00	0.85
$> 9 \rightarrow 4$	4.00	0.90
$6 \rightarrow 5$	64.00	0.22
$7 \rightarrow 5$	11.00	0.36
$8 \to 5$	3.00	0.45
$9 \rightarrow 5$	1.50	0.52
$> 10 \rightarrow 5$	5.00	0.55
$7 \rightarrow 6$	62.00	0.13
$8 \rightarrow 6$	12.00	0.22
$9 \rightarrow 6$	4.00	0.29
$10 \rightarrow 6$	2.00	0.33
$> 11 \rightarrow 6$	6.00	0.36

to decay and produce an electron, and ε_{det} is the detection probability of such an event. The signal, S, on the other hand, can be expressed as

$$S \approx d' \left(\frac{A_2}{A_1}\right) N_{stopped \,\mu^-} P_{laser-excited} P_{laser-excited \, reach \, the \, wall} \varepsilon_{det,X}. \tag{8}$$

Here, d' is the width of the laser-excited region, $P_{laser-excited}$ is the probability that the atoms in the region get excited by the laser, $P_{laser-excited \, reach \, the \, wall}$ is the probability that those that had been laser-excited will reach the wall of the target. Now, if we calculate the signal-to-background ratio, some of the parameters approximately cancel out:

$$\frac{S}{B} \approx \left(\frac{d'}{d}\right) \left(\frac{\varepsilon_{det,X}}{\varepsilon_{det,e^{-}}}\right) \frac{P_{laser-excited}P_{laser-excited reach the wall}}{\left(1 - e^{-\frac{300ns}{2200ns}}\right)} = \left(\frac{d'}{d}\right) \left(\frac{\varepsilon_{det,X}}{\varepsilon_{det,e^{-}}}\right) \frac{P_{laser}}{\left(1 - e^{-\frac{300ns}{2200ns}}\right)},\tag{9}$$

where $\frac{d'}{d}$ is the so-called overlap region, P_{laser} is a combined probability that the muonic atom will be laser excited and will reach the wall, and it is equal to $\sim 1\%$. Thus, the ratio $\frac{S}{B}$ is approximately 5×10^{-3} .

Combination of thin and thick scintillators Electrons and X-rays also can be partially distinguished by considering their total deposited energy. In fact, cascade events have energies up to 10 MeV while the energies of the electrons from the muon decay are distributed according to Fig. 5. A thick scintillator that completely absorbs the X-rays and the electrons could be used. A thin scintillator placed in front of the thick scintillator can be used to further distinguish between e^- and cascade events. Figure X shows the energy spectrum for cascade and μ -decay events in a 5-mm thick scintillator. By introducing an energy cut between 0.5-1 MeV, we can distinguish between cascade and e^- events.

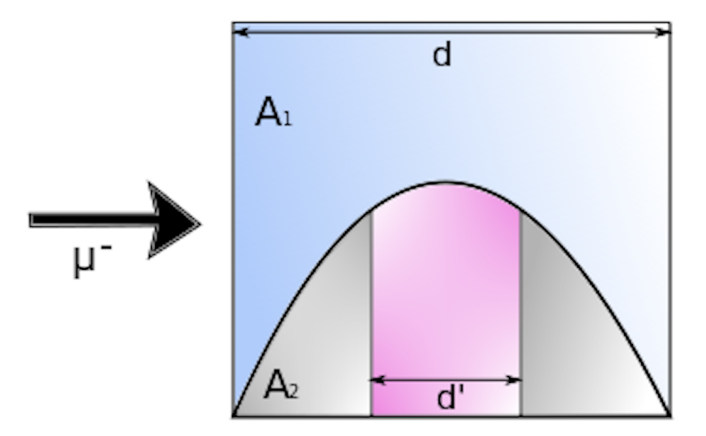
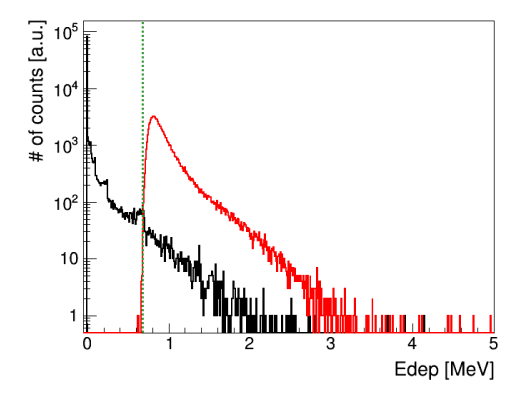
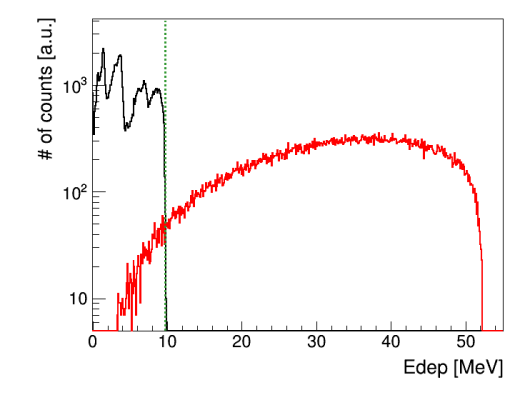


Figure 6: The density distribution of the μp atoms in the target. The x-axis points to the right and it represents the beam direction, whereas the y-axis is pointing downwards representing the time scale. The blue area A_1 shows the situation at the time t=0 ns. The almost parabolic grey area A_2 marks the loss normalisation background at the time when the laser enters the cavity t=1000 ns, whereas the pink region depicts the loss normalisation signal at the time t=1000 ns $+t_{excitation}$.



(a) Deposited energy in the 5-mm light plastic scintillator. A lower energy cut at 0.7 MeV [green dashed line] marks the intersection of different energy profiles and allows us to partially distinguish between the particles.



(b) Deposited energy in the 250-mm light plastic scintillator. An upper energy cut at 10 MeV [green dashed line] marks the intersection of different energy profiles and allows us to partially distinguish between the particles.

Figure 7: Deposited energy differences between electrons [red] and X-rays [black] in the 5-mm and 250-mm light plastic scintillator. The green dashed line shows a possible location for a cut to distinguish X-rays from electrons.

4 Interim results

Planar set-up This year various detector configurations have been simulated with the aim of optimising cascade detection efficiency while decreasing the misidentification of electrons as cascade events. One of the geometries is presented in Fig. 8. In the simulations, the effect

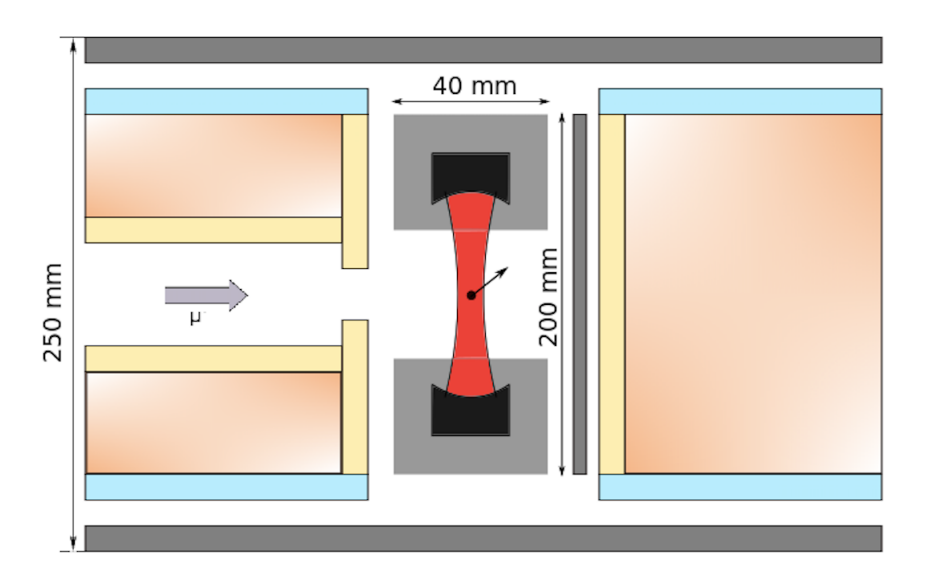
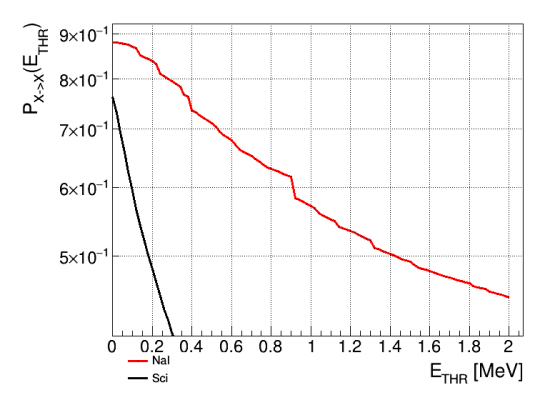
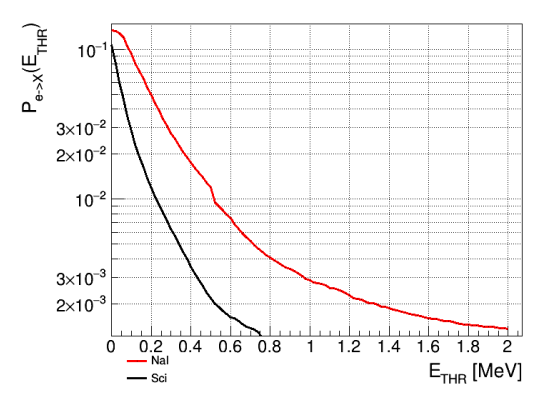


Figure 8: Planar detector set-up, with a target and a cavity in the center. Muons are incoming from the left, entering the cavity and getting excited by a laser light. The various thickness scintillating detectors (shown in yellow, orange, and blue) track the energy deposited in them.

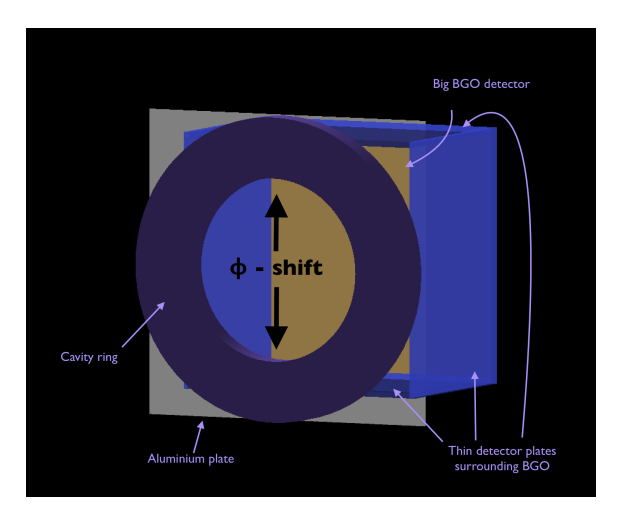
of the optical cavity and its mounting mechanics also has to be considered. The major source of electron misidentification arises from e^- impinging on the optical cavity and mounting mechanics that produce bremsstrahlung that is detected in the surrounding plastic scintillators and identified as cascade event (see Fig. 8). From this set-up we obtained a cascade event detection probability of $\approx 6.7 \times 10^{-1}$ when the energy cut in the thin scintillator is chosen to bet $0.6 \, \text{MeV}$ as can be seen in Fig. 9.



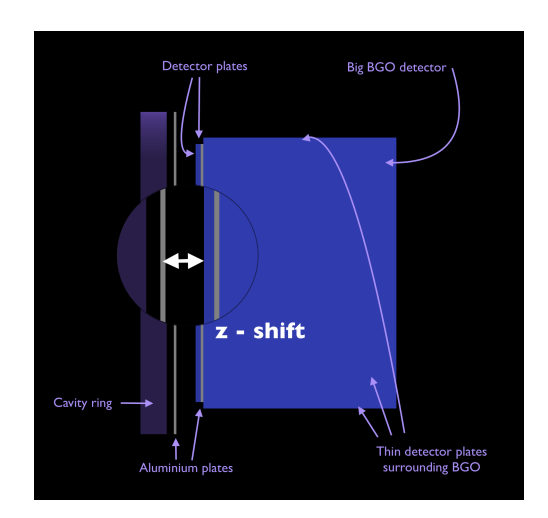


- (a) X-ray detection efficiency $P_{X\to X}$ versus a varying lower energy cut E_{THR} .
- (b) Probability that an electron is misidentified as a cascade $P_{e\to X}$ versus a lower energy cut E_{THR} .

Figure 9: X-ray detection efficiency $P_{X\to X}$ and electron misidentification as a cascade probability $P_{e\to X}$ versus the variable lower energy cut E_{THR} as obtained from the set-up shown in the Fig. 9. Red and black curves show how the results differ if we use sodium iodide or light plastic scintillation detectors, respectively.



(a) Φ -shift: changing the inner and outer diameters of the cavity mechanics (shown as a purple ring). A thin aluminium plate is placed behind the cavity representing a target wall. It is followed by a big BGO detector that is surrounded with plates of light plastic scintillation detectors from both sides, top, and the bottom.



(b) z-shift: moving the detectors away from the target. A lateral view to the planar-geometry detection scheme shows two aluminium plates with two thin light plastic scintillation detectors in between them. The big BGO scintillation detector and it surrounding light plastic scintillation detectors are shown on the right.

Figure 10: Optimisation of the ϕ - and z-shifts for the down-stream part of the detector with a planar geometry.

Optimisation of the ϕ - and z-shifts — In another set-up, where only the down-stream half of the detection system was simulated, the parameters were being optimised by varying the distance between the target cavity with the surrounding mechanics and the detectors. This variation was called the z-shift. At the same time, the inner radius of the cavity was also varied introducing the so-called ϕ -shift (see Fig. 10). It was found out that an optical cavity with a diameter of $\phi = 50$ -mm and a z-shift z = 0-mm produce a background at the level of 1×10^{-2} applying the 0.5 MeV lower energy cut. Therefore, an optical cavity of copper is strongly disfavoured. Fig. 11 shows the cascade event efficiency and electron misidentification as a X-ray probability for various ϕ - and z-shifts.

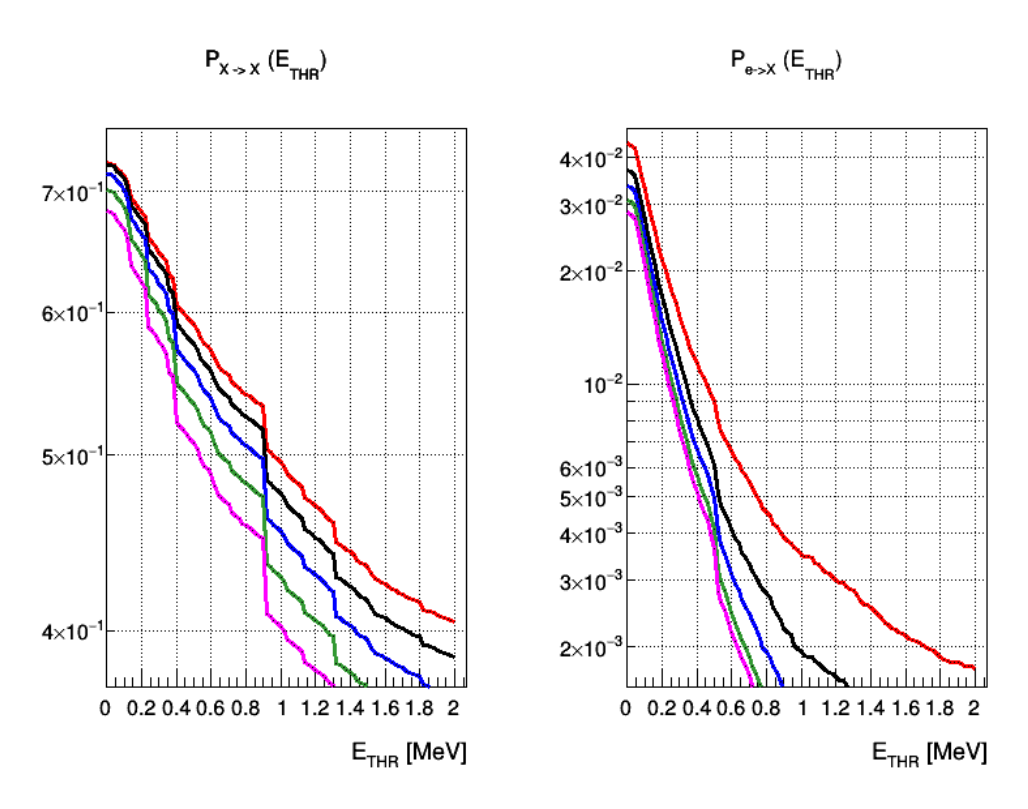


Figure 11: The variance in the X-ray detection efficiency $P_{X\to X}$ and in the electron misidentification as a X-ray probability $P_{e\to X}$ for a down-stream planar setup, plotted versus a lower energy threshold E_{THR} . Different curves are obtained introducing a fixed 50-mm ϕ -shift and 0-mm, 25-mm, 50-mm, 75-mm, and 100-mm z-shift.

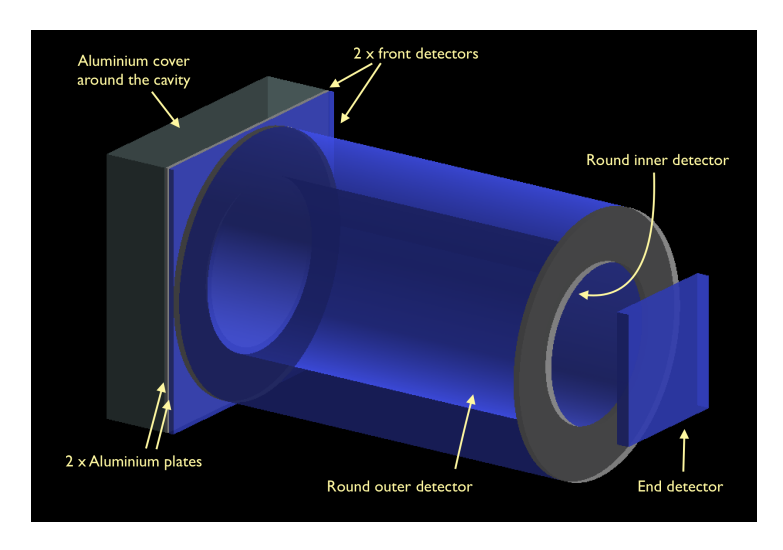


Figure 12: Magnetic setup: a hollow cylindrical scintillation detector in a constant 5 T magnetic field. Aluminium cover imitates a target area, where μp atoms are produced. The inner light plastic scintillation detector is topped up with an outer heavier-Z plastic scintillator or, instead, with a layer of aluminium. Between the target and the cylindrical detector there two thin scintillators surrounded by two aluminium plates. At the end of the cylinder [on the right] is yet another light plastic scintillator to detect the spiralling electrons exiting the setup.

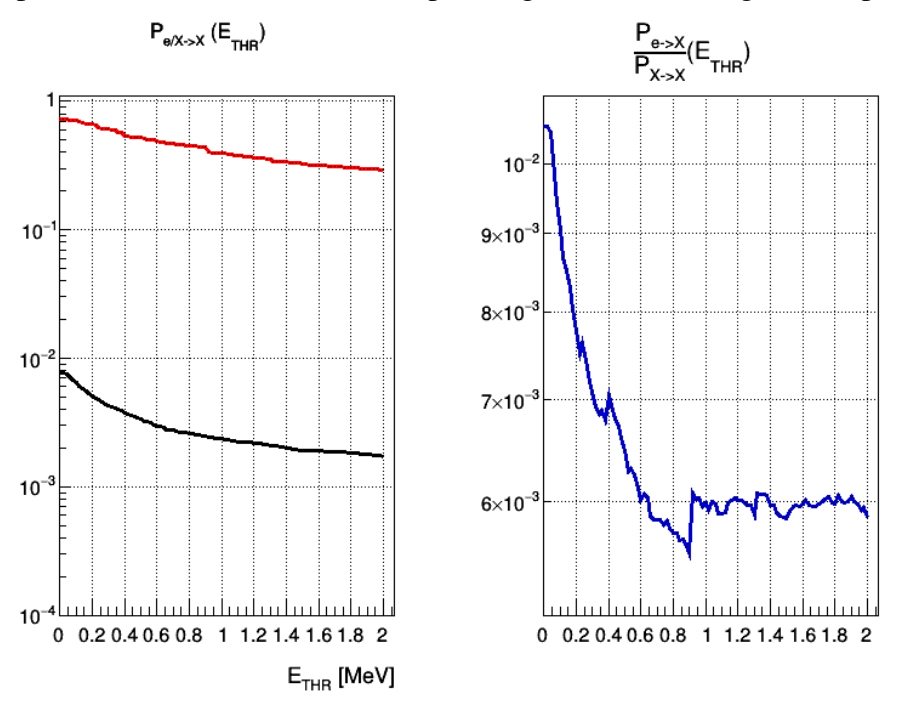


Figure 13: The e^- misidentification probability $P_{e\to X}$ [black] and the X-ray detection efficiency $P_{X\to X}$ [red] as obtained for the scenario with a magnetic setup.

Cylindrical detector in a magnetic field Another possibility of performing the experiment in a magnetic field was also studied. A hollow scintillating detector with a cylindrical geometry (Fig. 12) could be used so that e^- do not reach the detector. However, forcing the e^- to spiral into the magnetic field gives rise to an enhanced bremsstrahlung radiation when the e^- crosses the target walls. The left plot in the Fig. 13 shows the X-ray detection efficiency $P_{X\to X}$ [red] and electron misidentification probability $P_{e\to X}$ [black], whereas their relative ratio $\frac{P_{e\to X}}{P_{X\to X}}$ is shown on the right plot in blue.

5 Schedule of the research work

1st year [2017 - 2018] (done)

- Initial detection simulations
- Observation of the development of the single-frequency external cavity tapered amplifier laser system by the researchers from the National Tsing Hua University in Taiwan.
- Further detection simulations:
 - o Geometry, detector materials.
 - Event by event analysis.

2nd year [2018 - 2019]

- Advanced detection simulations:
 - Implementation of the advanced physical processes: nuclear capture and muon transfer, various cascade models.
- Writing of a technical summary of the detector simulations.
- Simulation of an alternative beam-line in $\pi e 5$ (if time permits).

• Measurements:

- Test of the detection system.
- o Measure the mean background, mean anti-coincidence detection efficiency.
- Measure stopping efficiencies.
- Initial work on Optical Parametric Oscillator (OPO), Optical Parametric Amplifier (OPA), and Difference-Frequency Generator (DFG):
 - o Check the various schemes and various crystal materials.
 - Simulation of the scheme and its optimisation.
 - Test of the scheme in the laboratory.

3rd year [2019 - 2020]

- Further work on OPO, OPA, and DFG:
 - o Characterisation of the pulse output.
 - Spectroscopy of the absorption lines.
- Contribution to the total setup:
 - o Development and installation of the data acquisition (DAQ) system.
 - Target finalisation and installation.
 - o Detector finalisation and installation.
 - Laser system's finalisation and installation.
- Beam-time, Physics run.
- Analysis of the beam-time data.
- Writing of the thesis.

6 Teaching activities

Previous teaching duties were:

- 2018 Teaching assistant for General Physics 2 (FS, Prof. K. Kirch)
- 2018 Proton Irradiation Facility (PIF) shift operator (HS, Dr. W. Hajdas)

Further activities are planned at the PIF at PSI and should occupy 10-13% of the total workload.

References

- [1] The CREMA collaboration. *Laser Spectroscopy of Muonic Atoms and Ions*. arXiv: 1609.03440v1, 2016.
- [2] Aldo Antognini, Franz Kottmann, François Biraben, Paul Indelicato, François Nez, and Randolf Pohl. *Theory of the* 2S 2P Lamb shift and 2S hyperfine splitting in muonic hydrogen. arXiv: 1208.2637v2, 2012.
- [3] The CREMA collaboration. *Proposal for an experiment at PSI: Hyperfine splittings in muonic hydrogen and 3He.* 2016.
- [4] R. N. Faustov and A. P. Martynenko. *Muonic hydrogen ground state hyperine splitting*. arXiv: hep-ph/0312116v2, 2004.
- [5] Franziska Hagelstein. *PhD thesis: Exciting nucleons in Compton scattering and hydrogen-like atoms*. arXiv: 1710.00874v1, 2017.

- [6] Xiaobing Xie et al. Injection-seeded single frequency $2.05~\mu m$ output by ring cavity optical parametric oscillator. Chinese Optics Letters, **15**(9), 2017.
- [7] G4beamline software,

http://www.muonsinternal.com/muons3/G4beamline.